 Related Commentary, page 1965

A stapled BIM peptide overcomes apoptotic resistance in hematologic cancers

James L. LaBelle,[1,2,3,4] Samuel G. Katz,[1,2,5,6] Gregory H. Bird,[1,2,4] Evripidis Gavathiotis,[1,2,4] Michelle L. Stewart,[1,2] Chelsea Lawrence,[1,2] Jill K. Fisher,[1,2] Marina Godes,[1,2] Kenneth Pitter,[1,2] Andrew L. Kung,[1,2,3,4] and Loren D. Walensky[1,2,3,4]

[1]Department of Pediatric Oncology and [2]Program in Cancer Chemical Biology, Dana-Farber Cancer Institute, Boston, Massachusetts, USA. [3]Division of Hematology/Oncology, Children's Hospital, Boston, Massachusetts, USA. [4]Department of Pediatrics and [5]Department of Pathology, Harvard Medical School, Boston, Massachusetts, USA. [6]Department of Pathology, Brigham and Women's Hospital, Boston, Massachusetts, USA.

Cancer cells subvert the natural balance between cellular life and death, achieving immortality through pathologic enforcement of survival pathways and blockade of cell death mechanisms. Pro-apoptotic BCL-2 family proteins are frequently disarmed in relapsed and refractory cancer through genetic deletion or interaction-based neutralization by overexpressed antiapoptotic proteins, resulting in resistance to chemotherapy and radiation treatments. New pharmacologic strategies are urgently needed to overcome these formidable apoptotic blockades. We harnessed the natural killing activity of BCL-2–interacting mediator of cell death (BIM), which contains one of the most potent BH3 death domains of the BCL-2 protein family, to restore BH3-dependent cell death in resistant hematologic cancers. A hydrocarbon-stapled peptide modeled after the BIM BH3 helix broadly targeted BCL-2 family proteins with high affinity, blocked inhibitory antiapoptotic interactions, directly triggered proapoptotic activity, and induced dose-responsive and BH3 sequence–specific cell death of hematologic cancer cells. The therapeutic potential of stapled BIM BH3 was highlighted by the selective activation of cell death in the aberrant lymphoid infiltrates of mice reconstituted with BIM-deficient bone marrow and in a human AML xenograft model. Thus, we found that broad and multimodal targeting of the BCL-2 family pathway can overcome pathologic barriers to cell death.

Introduction

The BCL-2 family interaction network lies at the crossroads of the cell's life-death decision (1, 2). Among the oncogenic signals that drive the development and maintenance of cancer, the pathologic reprogramming of the BCL-2 family interaction network has emerged as a formidable barrier to modern day anticancer treatment. Antiapoptotic members of the BCL-2 family contain a surface hydrophobic groove that can bind, sequester, and neutralize the critical BH3 death domains of proapoptotic members (3). Small molecules, such as ABT-737 and ABT-263, that selectively inhibit the antiapoptotic proteins BCL-2 and BCL-X_L induce apoptosis of tumors that are especially dependent upon this subset of survival proteins (4, 5). However, the compounds are rendered ineffective by cellular expression of alternate antiapoptotic proteins, such as MCL-1 and BFL1/A1, which lie outside the molecules' range of binding specificity or by the relative or absolute absence of proapoptotic effectors, such as BAX and BAK (6, 7). Thus, a pharmacologic quest is underway to develop next-generation agents that simulate broader spectrum BH3-dependent killing activities and effectively deactivate the deflector shields of relapsed and refractory cancers.

Chief among the killer BH3-only proteins, Bcl-2–interacting mediator of cell death (BIM) exhibits the most broad-ranging BCL-2 protein interactions, engaging all of the antiapoptotic proteins with high affinity (8, 9) and also directly triggering death effectors, such as BAX (10, 11). A recent genetic analysis elegantly demonstrated that only BIM BH3, but not other BH3 sequences inserted into the BIM protein, could rescue the leukocyte accumulation and autoimmune phenotype of *Bim*$^{-/-}$ mice (12). These data emphasize the unique killing potency of BIM BH3, which may derive from its higher-affinity interactions with antiapoptotics, dual capacity to block antiapoptotics and directly activate proapoptotics, and/or engagement of yet uncharacterized proteins that contribute to induction of cell death. From a clinical translational standpoint, BIM induction appears essential for cell death responses to a host of chemotherapeutic agents, and BIM suppression by genetic deletion, miRNA-based suppression, or protein interaction-based neutralization or degradation accounts for the emergence of drug resistance (13–15). Therefore, harnessing the BIM BH3 helix to promote a death response and, in particular, chemical replacement of this death functionality, in the context of drug resistance, are logical pharmacologic goals (16–18).

We previously developed stabilized α helix of BCL-2 domains (SAHBs), which are structurally stable, protease-resistant, and cell-permeable compounds capable of targeting BCL-2 family proteins with high affinity (19, 20). Here, we examined the pharmacologic potential of BIM $SAHB_A$, a stapled BIM BH3 helix that contains an *i*, *i+4* all-hydrocarbon crosslink spanning positions 154 and 158 (designated "*A*"), to restore cell death in the context of formidable and clinically relevant apoptotic resistance. We found that BIM $SAHB_A$ reactivates cell death in a BH3 sequence–dependent fashion in vitro and in vivo and, importantly, preferentially affects cells driven by a deregulated apoptotic pathway.

Results

BIM $SAHB_A$ binds with high affinity to a broad range of BCL-2 family proteins. To explore the breadth of BIM BH3 activity, we generated a hydrocarbon-stapled BIM BH3 helix (amino acids 146–166) (19)

Conflict of interest: Loren D. Walensky is a scientific advisory board member and consultant for Aileron Therapeutics.

Citation for this article: *J Clin Invest.* 2012;122(6):2018–2031. doi:10.1172/JCI46231.

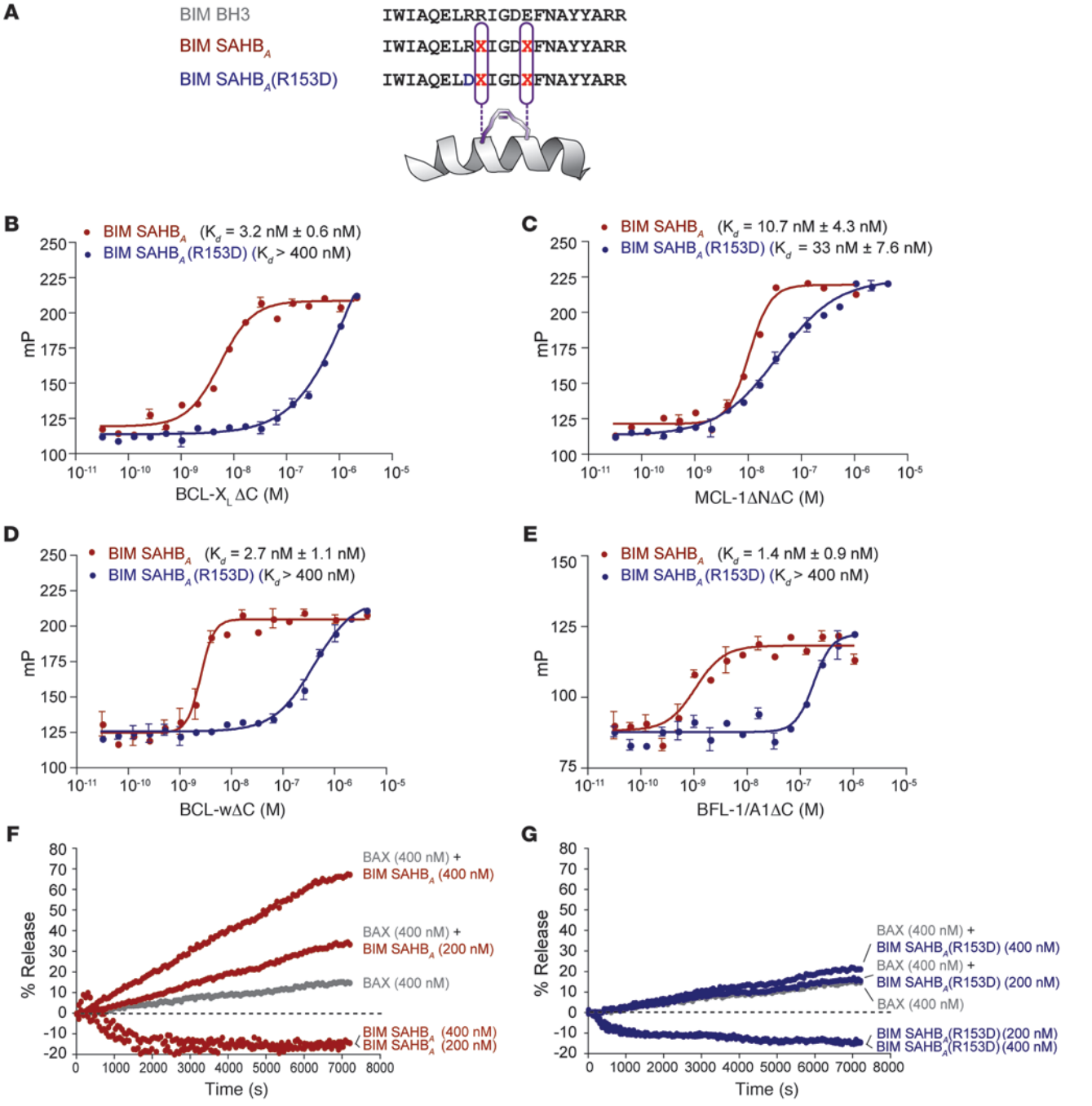

Figure 1

Broad-spectrum BCL-2 family binding activity of a stapled BIM BH3 helix. (**A**) Sequence composition of BIM SAHB$_A$ and its R153D mutant. "X" denotes the position of the nonnatural amino acid within each peptide. (**B**–**E**) BIM SAHB$_A$ binds to a broad range of antiapoptotic targets with high affinity. R153D mutagenesis shifts the isotherms to the right, reflecting the impairment of binding activity. Data are mean ± SEM for experiments performed at least in triplicate. mP, units of millipolarization. (**F** and **G**) BIM SAHB$_A$ triggers dose-responsive BAX-mediated liposomal release, whereas the R153D mutant has no effect. The liposomal release assays were performed in triplicate with similar results.

and a negative control peptide based on an R153D reverse polarity mutation within the core BH3 sequence (ref. 10, Figure 1A, and Supplemental Table 1; supplemental material available online with this article; doi:10.1172/JCI46231DS1). Circular dichroism analysis demonstrated that BIM SAHB$_A$ and BIM SAHB$_A$(R153D) exhibit enhanced α-helical structure in solution compared with that of the corresponding unmodified BIM BH3 peptide (ref. 19 and Supplemental Figure 1), effectively recapitulating the native structure of this domain when bound to apoptotic targets (21–23). Equilibrium fluorescence polarization (FP) binding analysis using FITC-βAla-BIM SAHB$_A$ peptides and recombinant and tagless BCL-X$_L$ΔC, MCL-1ΔNΔC, BCL-wΔC, and BFL1/A1ΔC revealed

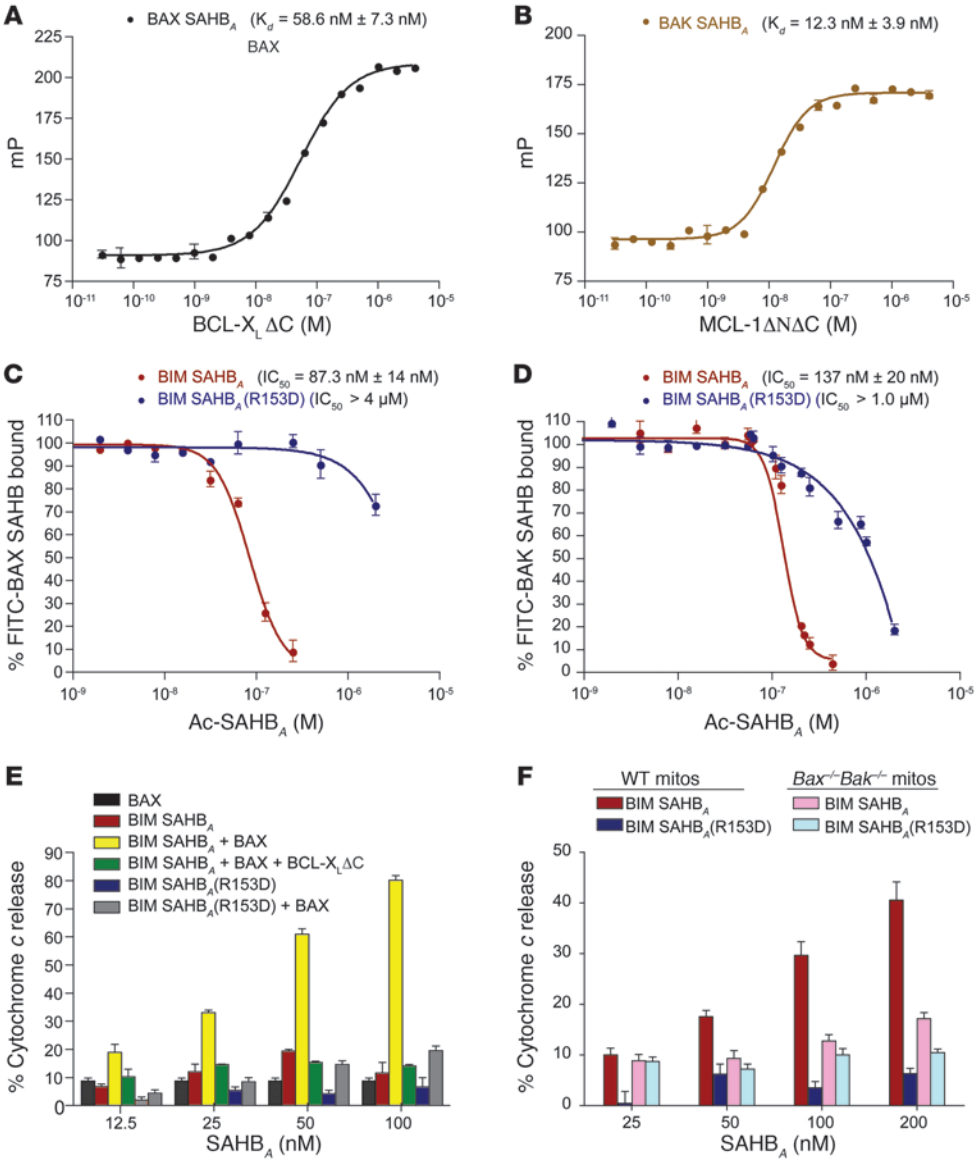

Figure 2
BIM SAHB$_A$ dissociates inhibitory antiapoptotic interactions and directly triggers BAX/BAK-dependent mitochondrial cytochrome *c* release. (**A** and **B**) The antiapoptotic proteins BCL-X$_L$ΔC and MCL-1ΔNΔC, respectively, sequester the proapoptotic BH3 helices of BAX and BAK in high-affinity complexes. (**C** and **D**) BIM SAHB$_A$ effectively dissociates the inhibitory complexes, whereas R153D mutagenesis markedly impairs competitive binding. (**E**) BAX/BAK-deficient MLM (mouse liver mitochondria) undergo cytochrome *c* release in response to combination treatment with recombinant BAX (50 nM) and increasing doses of BIM SAHB$_A$. The specificity of action is highlighted by (a) blockade of the effect by added recombinant BCL-X$_L$ΔC (2 μM), (b) loss of activity upon R153D mutagenesis, and (c) the inability of BAX and BIM SAHB$_A$s to influence cytochrome *c* release when administered as single agents. (**F**) To monitor BAK-dependent cytochrome *c* release, WT MLM that contain native BAK were exposed to BIM SAHB$_A$ and its R153D mutant. BIM SAHB$_A$ triggered BH3 sequence–dependent and BAK-dependent cytochrome *c* release, with little to no effect on the corresponding BAX/BAK-deficient MLM in the 0–200 nM dosing range. Data are mean ± SEM for experiments performed at least in triplicate.

1–11 nM K_d values for BIM SAHB$_A$ across antiapoptotic targets, whereas R153D mutagenesis consistently reduced binding activity (Figure 1, B–E). We previously demonstrated, both by FP (19) and NMR (10), that BIM SAHB$_A$ and an analog optimized for structural analysis (amino acids 145–164), respectively, also bind to proapoptotic BAX. In contrast to the static interaction between BH3 domains and their canonical binding pocket on antiapoptotic proteins, the BIM BH3 helix engages a geographically distinct BH3-binding site on BAX (10), triggering a major structural reorganization that underlies the dynamic BAX activation process (24). Indeed, combining BIM SAHB$_A$ with recombinant BAX triggered dose-responsive BAX-mediated liposomal release, linking the direct binding interaction to BAX's transformation from an inactive monomer to a functional pore (Figure 1F). Importantly, the single R153D point mutation at the binding interface abrogated the BAX-triggering activity of BIM SAHB$_A$ in this assay (Figure 1G). As a further measure of specificity, BIM SAHB$_A$–triggered and BAX-mediated liposomal release was blocked in the presence of antiapoptotic proteins BCL-X$_L$ΔC, MCL-1ΔNΔC, BCL-wΔC, and BFL-1/A1ΔC (Supplemental Figure 2). Thus, BIM SAHB$_A$ engages a diversity of multidomain BCL-2 family proteins, consistent with the established broad-spectrum interaction profile of native BIM protein (8–10, 19).

BIM SAHB$_A$ blocks antiapoptotic sequestration of the BAX/BAK BH3 helices and triggers BAX/BAK-dependent mitochondrial cytochrome c release. An established paradigm for overcoming the apoptotic blockade of refractory cancer involves pharmacologic derepression of sequestered proapoptotic BCL-2 family members by competitive binding to antiapoptotic targets (8, 25–27). To explore the capacity of BIM SAHB$_A$ to function as a derepressor compound, we performed competition assays using FITC-βAla-BAX SAHB$_A$/BCL-X$_L$ΔC (K_d, 58.6 nM) and FITC-βAla-BAK SAHB$_A$/MCL-1ΔNΔC (K_d, 12.3 nM) (Figure 2, A and B). In each case, BIM SAHB$_A$ dose responsively competed with the death effector BH3 helix for antiapoptotic binding, whereas BIM SAHB$_A$(R153D) was a relatively weak competitor (Figure 2, C and D).

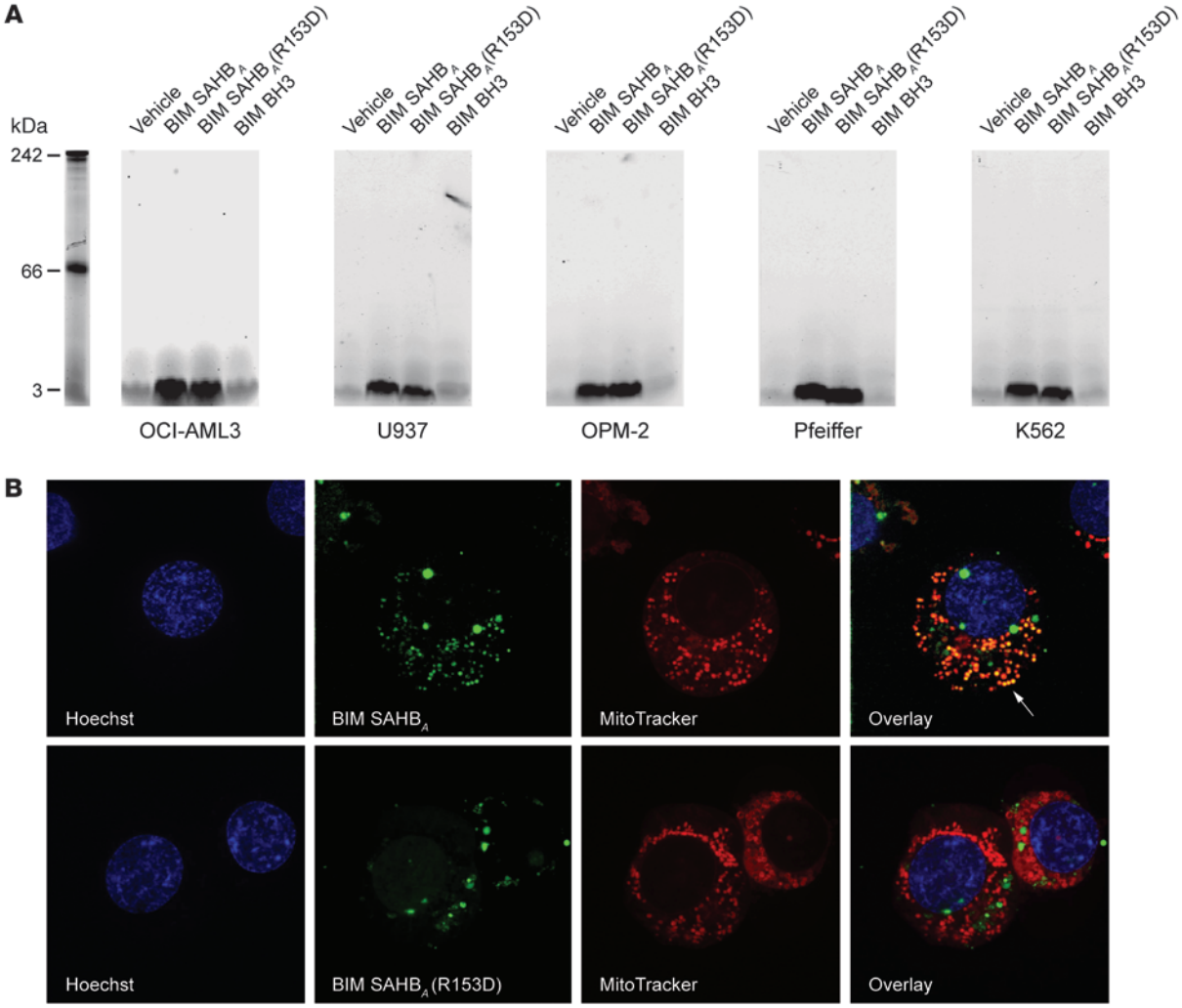

Figure 3
Cellular uptake and localization of BIM SAHB$_A$s. (**A**) Cultured cancer cells were exposed to FITC derivatives of BIM BH3 peptides (1 μM) for 2 hours, followed by centrifugation, trypsinization, washing, lysate preparation, electrophoresis, and fluorescence detection. FITC-BIM SAHB$_A$ and its R153D point mutant were present at similar levels in the cellular lysates, whereas no uptake was observed for the unmodified FITC-BIM BH3 peptide. (**B**) Live cell confocal microscopy of U937 cancer cells treated with FITC-BIM SAHB$_A$s (1 μM, 2 hours) demonstrated the uptake and intracellular distribution of the peptides. FITC-BIM SAHB$_A$, but not the impaired R153D mutant, largely colocalizes with mitochondria, the site of BCL-2 family targets. Nuclei (Hoechst), SAHBs (FITC), mitochondria (MitoTracker), and the BIM SAHB$_A$/mitochondria colocalization (FITC/MitoTracker) are shown in blue, green, red, and yellow, respectively. An example of the BIM SAHB$_A$/mitochondria colocalization is highlighted by the white arrow. Original magnification, ×100.

To examine the functional impact of the broad targeting activity of BIM SAHB$_A$ in the mitochondrial context, we performed cytochrome *c* release assays in the presence of BAX (*Alb-cre^{pos}Bax$^{fl/-}$Bak$^{-/-}$* mouse liver mitochondria [MLM] with added recombinant BAX) or BAK (WT MLM) or without either effector protein (*Alb-cre^{pos}Bax$^{fl/-}$Bak$^{-/-}$* MLM). Applying a 0–200 nM dosing range, BIM SAHB$_A$ selectively triggered recombinant BAX- and native BAK-dependent cytochrome *c* release, with little to no release observed with BIM SAHB$_A$(R153D) or in the absence of BAX and BAK (Figure 2, E and F). Thus, we demonstrate that low nanomolar BIM SAHB$_A$ has the capacity to broadly engage BCL-2 family targets to selectively trigger BH3 sequence–dependent and BAX/BAK-dependent mitochondrial apoptosis.

BIM SAHB$_A$ activates caspase-3/7 and induces cell death in resistant hematologic cancer cells. We examined the utility of BIM SAHB$_A$ in overcoming the apoptotic blockades of refractory cancer by testing a series of hematologic cancer cell lines that are relatively resistant to ABT-737 (5, 6, 28, 29), a selective BCL-2/BCL-X$_L$ inhibitor whose activity is dampened by cellular expression of antiapoptotic proteins that lie outside its binding spectrum (4, 6, 7, 30). We first documented that BIM SAHB$_A$ and its mutant derivative exhibit dose-equivalent uptake by the panel of cancer cell lines, which included OCI-AML3 (acute myeloid leukemia [AML]), U937 (monocytic leukemia/lymphoma), OPM-2 (multiple myeloma), Pfeiffer (diffuse large B cell lymphoma), and K562 (chronic myelogenous leukemia) cells (Figure 3A). Cultured cells were treated with vehicle

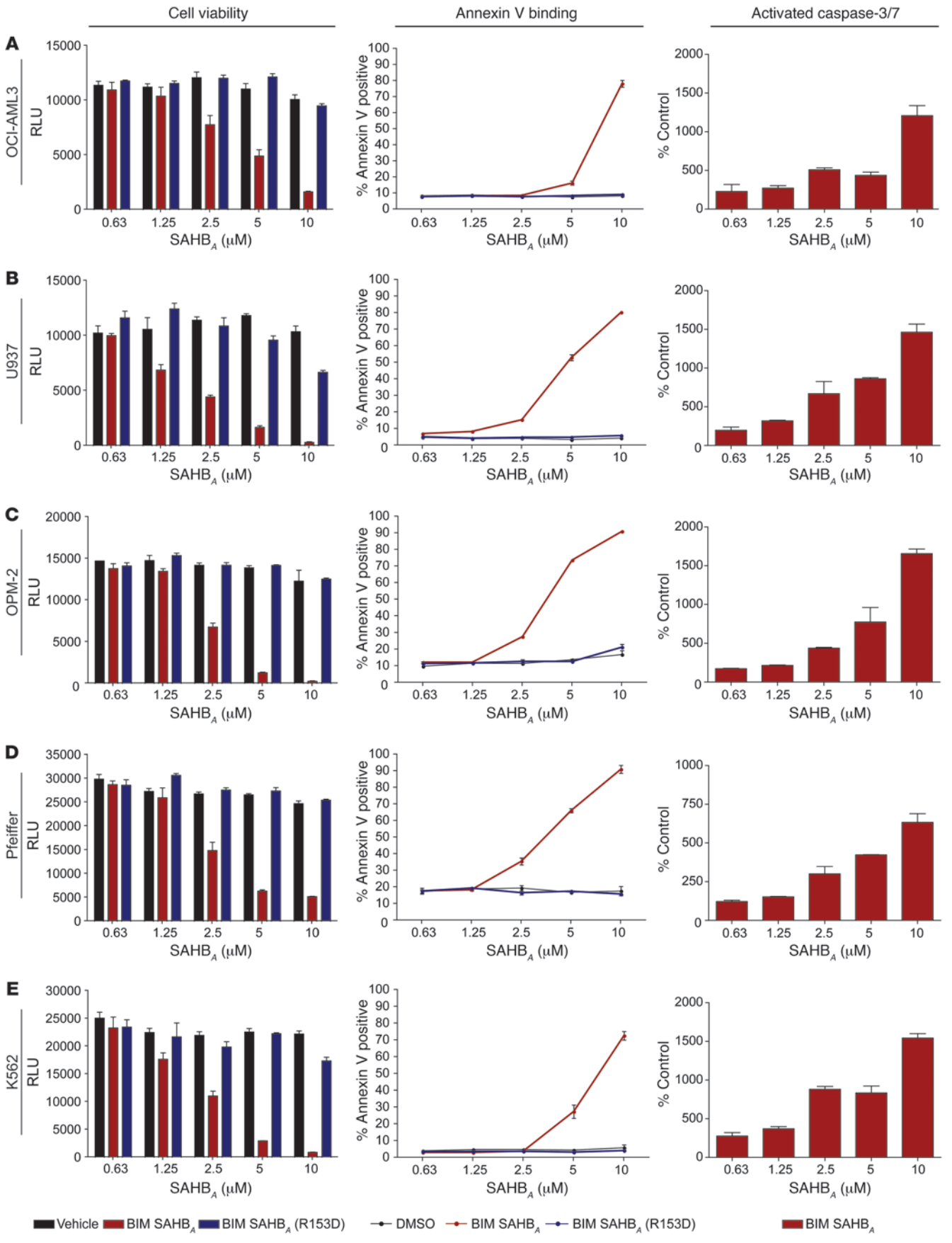
Cell viability
Annexin V binding
Activated caspase-3/7
A
OCI-AML3
B
U937
C
OPM-2
D
Pfeiffer
E
K562
RLU
% Annexin V positive
% Control
SAHB$_A$ (μM)
0.63
1.25
2.5
5
10
Vehicle
BIM SAHB$_A$
BIM SAHB$_A$ (R153D)
DMSO

Figure 4
Sequence-dependent cytotoxicity of BIM $SAHB_A$ in hematologic cancer cells resistant to selective BCL-2/BCL-X_L inhibition. BIM $SAHB_A$ dose responsively reduces the viability of (**A**) OCI-AML3, (**B**) U937, (**C**) OPM-2, (**D**) Pfeiffer, and (**E**) K562 cancer cells, as measured at 24 hours by CellTiter-Glo assay (left column). R153D mutagenesis markedly impairs the cytotoxic activity of BIM $SAHB_A$. Cells exposed to BIM $SAHB_A$, but not its R153D mutant, exhibit dose-dependent annexin V binding at 6 hours after treatment, as monitored by FACS analysis (middle column). The negative effect of BIM $SAHB_A$ on cancer cell viability correlates with dose-responsive activation of caspase-3/7, as assessed by monitoring the cleavage of proluminescent caspase-3/7 substrate at 6 hours after treatment (right column). Data are mean ± SEM for experiments performed at least in triplicate. RLU, relative luminescence units.

or FITC-derivatized BH3 peptides (1 μM) in serum-free media for 2 hours, followed by centrifugation, trypsinization (to digest surface proteins and thereby eliminate potential nonspecific surface binding), washing, lysate preparation, electrophoresis, and fluorescence scan detection. Importantly, FITC-BIM $SAHB_A$ and FITC-BIM $SAHB_A$(R153D) were present at similar levels within the cellular lysates, whereas the vehicle- and unmodified FITC-BIM BH3–treated cells showed no signal (Figure 3A). Live cell confocal microscopy of FITC-SAHB–treated cells further confirmed cellular uptake of the stapled peptides (Figure 3B). Whereas FITC-BIM $SAHB_A$ largely colocalized with mitochondria, the predominant site of BCL-2 family targets (31), the R153D point mutant that exhibits substantially impaired binding activity showed little to no such colocalization. We further confirmed that at the micromolar dosing levels used for cellular studies, BIM $SAHB_A$ peptides were solubilized as uniform, monomeric species, as assessed by gel filtration chromatography (Supplemental Figure 3).

Cancer cells were then exposed to serial dilutions of vehicle, BIM $SAHB_A$, and BIM $SAHB_A$(R153D), and the effect of treatment was monitored by cell viability assay, annexin V binding FACS analysis, and caspase-3/7 activation assay (Figure 4). In each case, BIM $SAHB_A$ impaired cancer cell viability in a dose-responsive and sequence-dependent manner (IC_{50}, 1.8–3.4 μM), an effect that correlated with both annexin V positivity and caspase-3/7 activation. When applied to nonmalignant cells that also demonstrated efficient uptake of BIM $SAHB_A$ (Supplemental Figure 4), such as the human fibroblast cell line WS1 and WT and *Bax*$^{-/-}$*Bak*$^{-/-}$ (DKO) mouse embryo fibroblasts (MEFs), neither BIM $SAHB_A$ nor BIM $SAHB_A$(R153D) had any cytotoxic or caspase-3/7 activation effects in the same 0–10 μM dosing range (Figure 5). Only when increasing the dose to 20 μM do we begin to observe a decrease in WS1 cell viability, which coincides with caspase-3/7 activation (Supplemental Figure 5A); in adherent MEFs, this dose escalation does not impact cell viability, but a mild elevation in caspase-3/7 activation is observed in WT MEFs but not DKO MEFs, consistent with a BAX/BAK-dependent proapoptotic mechanism (Supplemental Figure 5, B and C). To confirm that the relative lack of toxicity of human BIM $SAHB_A$ in murine fibroblasts did not derive from cross-species variation, we repeated the experiment with the corresponding murine BIM $SAHB_A$s (Supplemental Table 1) and obtained similar results (data not shown). Thus, these data indicate that at low micromolar dosing, BIM $SAHB_A$ activates the death pathway in a variety of hematologic cancer cells that are otherwise resistant to selective BCL-2/BCL-X_L inhibition (6, 7). Importantly, the relative resistance of nonmalignant fibroblasts to BIM $SAHB_A$ treatment suggested that a therapeutic window may exist for BIM BH3 replacement in vivo, with preferential toxicity to cells driven by deregulated apoptosis.

Mechanism of BIM $SAHB_A$–induced cytotoxicity. To further probe the protein interaction-based mechanism of BIM $SAHB_A$ activity, we treated OCI-AML3 cells with BIM SAHBs (0–10 μM) and monitored for disruption of the inhibitory MCL-1/BAK complex (32) and conversion of BAX to its conformationally activated form (10) by immunoprecipitation with antibodies to MCL-1 and the BAX activation epitope (6A7) (33), respectively. Cellular treatment with BIM $SAHB_A$, using the same dose range that induced cytotoxicity, annexin V binding, and caspase-3/7 activation (Figure 4), triggered both dose-responsive dissociation of MCL-1/BAK (Figure 6A) and exposure of the BAX activation epitope (Figure 6B), consistent with pharmacologic induction of the mitochondrial apoptotic pathway. Importantly, BIM $SAHB_A$(R153D) showed no such effects. In accordance with the observed BIM $SAHB_A$–induced biochemical changes, OCI-AML3 cells likewise manifested the morphologic features of apoptosis, as reflected by cellular contraction, chromatin condensation and marginalization, and nuclear fragmentation of Wright-Giemsa–stained cytospun cells (Figure 6C).

Tumor suppressive activity of BIM $SAHB_A$ as a single agent and in combination. To extend these findings to an in vivo context, we tested the efficacy of BIM $SAHB_A$ in an OCI-AML3 human xenograft model (34). OCI-AML3-LucNeo cells (5×10^6 cells) were implanted subcutaneously with 30% Matrigel into the right hind flank of 6-week-old female NOD scid gamma (NSG) mice. Mice with equivalent disease, as determined by bioluminescent imaging on day 8 after inoculation, were divided into 2 groups ($n = 7$ per arm), treated daily with either i.v. vehicle (5% DMSO/D5W) or BIM $SAHB_A$ (25 mg/kg), and imaged on days 0, 4, 7, and 10. Throughout the treatment period, mice receiving BIM $SAHB_A$ manifested a statistically significant suppression of tumor growth compared with that of vehicle-treated animals, as reflected by an approximately 50% decrease in relative bioluminescence (2-way ANOVA, $P = 0.018$) (Figure 6D).

We next explored whether the single agent activity of BIM $SAHB_A$ could be combined with other proapoptotic agents to enhance the antitumor response. BIM $SAHB_A$ was combined with either TRAIL, an extrinsic apoptotic pathway stimulus, or ABT-737, an intrinsic apoptotic pathway stimulus, in synergy analyses (35) performed on OCI-AML3 cells. The cancer cells were treated with serial dilutions of BIM $SAHB_A$, TRAIL, or ABT-737 or the combination of BIM $SAHB_A$ and TRAIL or BIM $SAHB_A$ and ABT-737, followed by viability assay at 24 hours (Figure 7, A and B). In each case, synergy was observed, as reflected by combination indices of less than 1 at the 50%, 75%, and 90% effective doses. To determine whether a drug combination could enhance the antitumor activity of BIM $SAHB_A$ in vivo, we repeated the OCI-AML3 xenograft study ($n = 8$ per arm), examining the impact of adding the orally bioavailable BCL-2/BCL-X_L inhibitor ABT-263 (5, 36) (100 mg/kg/d per orem [PO]) to either BIM $SAHB_A$ or its point-mutant control BIM $SAHB_A$(R153D) (25 mg/kg/d i.v.). Mice were treated for 15 days with vehicle, the single agent SAHB, or the combination of SAHB with ABT-263, and bioluminescence was measured on days 0, 3, 7, 10, 13, and 16. As previously observed (Figure 6D), single agent BIM $SAHB_A$ suppressed tumor growth throughout the treatment period ($P = 0.0299$) (Figure 7C). Single R153D point mutagenesis abrogated this effect, with BIM $SAHB_A$(R153D) treat-

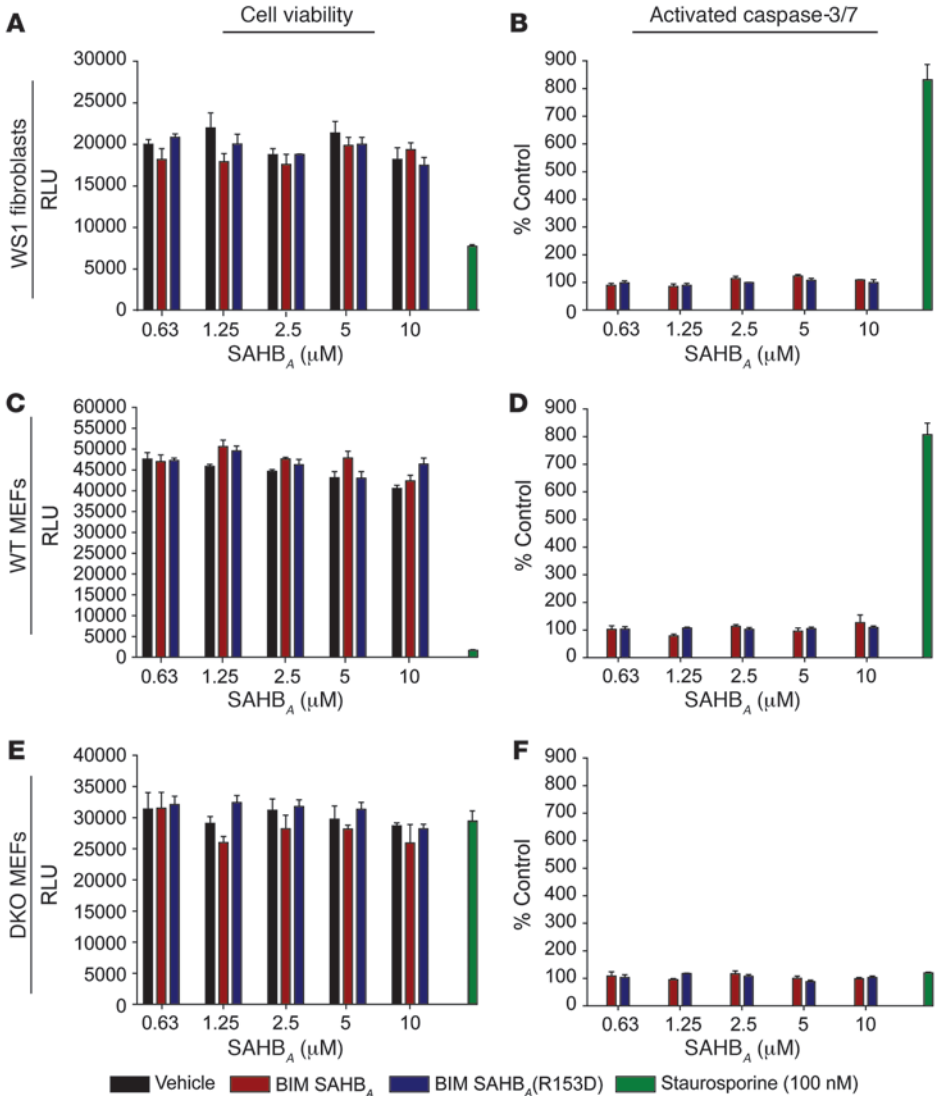

Figure 5
Viability of human and mouse fibroblasts exposed to BIM SAHB$_A$ peptides. WS1 human fibroblasts showed no response to BIM SAHB$_A$ peptides (0–10 μM), as assessed by (**A**) viability and (**B**) caspase-3/7 activation assays performed at 24 and 6 hours after treatment, respectively. Staurosporine (100 nM), which impaired viability and induced caspase-3/7 activation, served as a positive control. Adherent WT and DKO MEFs likewise showed no response to BIM SAHB$_A$ treatment in this dose range, as assessed by (**C** and **E**) viability and (**D** and **F**) caspase-3/7 activation assays. As a positive control, (**C** and **D**) staurosporine (100 nM) triggered caspase-3/7 activation and reduced viability of WT MEFs, (**E** and **F**) whereas DKO MEFs exhibited relative resistance to staurosporine with no caspase-3/7 activation, as reported previously (50). Data are mean ± SEM for experiments performed at least in triplicate.

ment showing no statistically significant tumor suppressive activity (P = 0.3934). The addition of ABT-263 to BIM SAHB$_A$ yielded the most significant antitumor response (P = 0.0009), whereas combining ABT-263 with BIM SAHB$_A$(R153D) did not achieve a significant antitumor effect (P = 0.1982) (Figure 7C). Importantly, neither BIM SAHB$_A$ nor BIM SAHB$_A$/ABT-263 combination treatment adversely affected peripheral white blood cell counts (Supplemental Figure 6), and no weight loss was observed among the treatment groups (Figure 7D). Taken together, the in vivo efficacy data are consistent with BIM BH3 sequence–dependent antitumor activity, both as a single agent and in combination with ABT-263, in an otherwise aggressive and relatively resistant xenograft model of human AML.

Therapeutic potential of BIM BH3 replacement. To explore the in vivo capacity of BIM SAHB$_A$ to selectively reactivate the death pathway in cells driven by a formidable genetic apoptotic blockade, we transplanted the bone marrow (2×10^6 cells) from *Bim*$^{-/-}$ mice (37) into *Rag2*$^{-/-}$*gc*$^{-/-}$ recipients, yielding uniform cohorts of mice manifesting the immune cell accumulation of native *Bim*$^{-/-}$ mice (38), as evidenced by organ infiltrates (Figure 8A), hypergammaglobulinemia (Supplemental Figure 7A), and splenomegaly (Supplemental Figure 7B) evaluated at 19, 15, and 12 weeks post transplant, respectively. Histologic analysis of solid organs, such as the kidney and liver by H&E stain and anti-B220 immunohistochemistry, documented the presence of pathologic B cell infiltrates throughout the tissues (Figure 8A). Post transplant day–matched mouse cohorts (n = 4) were treated with daily i.v. injections of vehicle (5% DMSO/D5W) or 10 mg/kg of murine BIM SAHB$_A$s for 5 days, followed by necropsy and histologic analysis. The relative degree of apoptosis induction was measured by TUNEL staining, which revealed a statistically significant increase in TUNEL positivity in the liver and kidney infiltrates of BIM SAHB$_A$–treated mice compared with that in vehicle- and BIM SAHB$_A$(R153D)–treated animals (Figure 8, B–D). Importantly, no increase in TUNEL staining was observed in the surrounding normal liver and kidney parenchyma of BIM SAHB$_A$–treated mice (Figure 8, B, C, and E). Of note, *Bim*$^{-/-}$ bone marrow–reconstituted *Rag2*$^{-/-}$*gc*$^{-/-}$ mice treated with BIM SAHB$_A$ for 5 days also manifested a trend toward lower spleen weight and spleen weight per body weight compared with that of vehicle- and BIM SAHB$_A$(R153D)–treated animals (Supplemen-

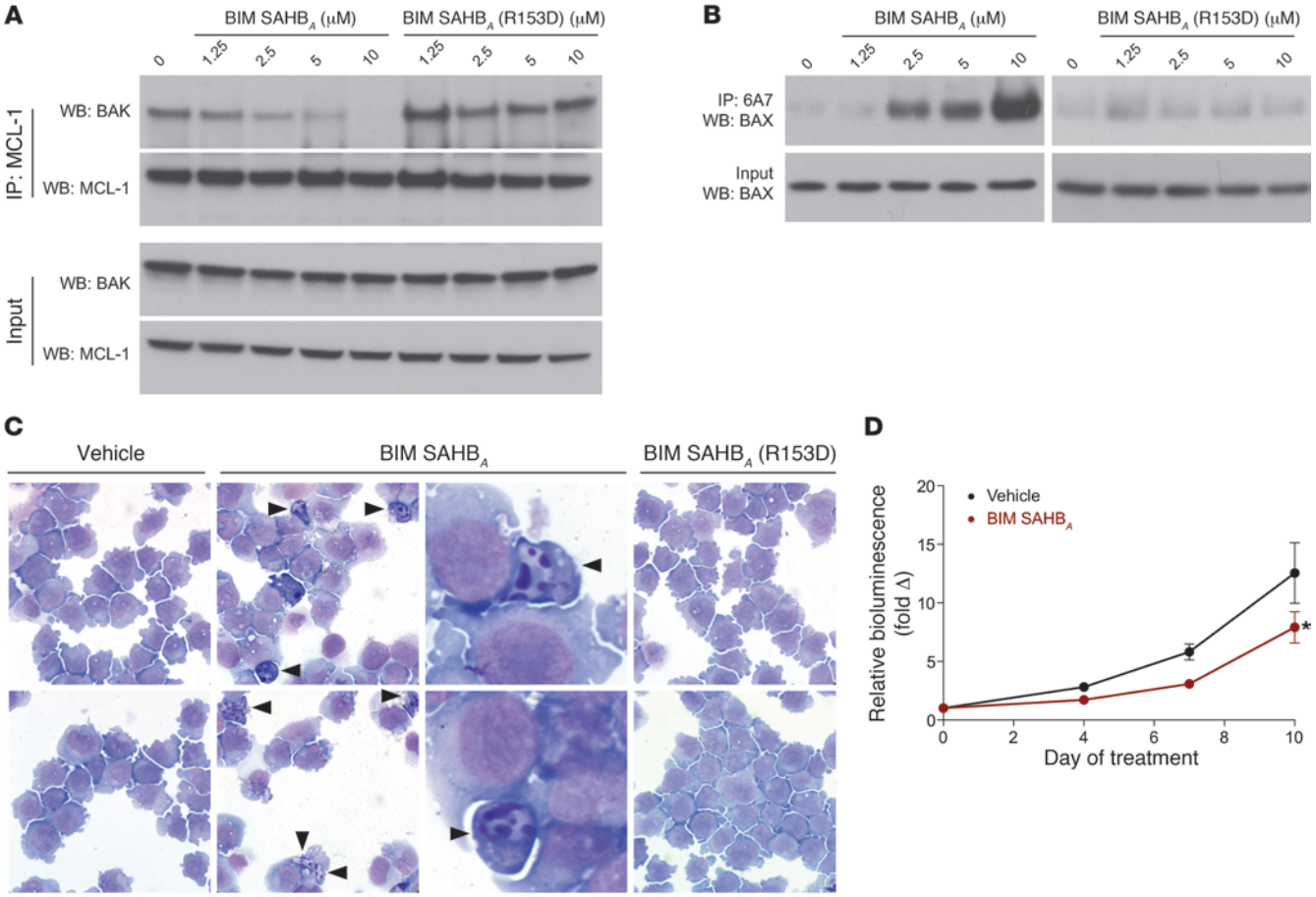

Figure 6

BIM SAHB$_A$ treatment induces biochemical and morphological changes that reflect a proapoptotic mechanism of action. (**A**) OCI-AML3 cells treated with BIM SAHB$_A$ (0–10 μM) manifest dose-responsive dissociation of the native BAK/MCL-1 complex, as assessed by MCL-1 immunoprecipitation and anti-BAK Western analysis. No effect is observed upon treatment with BIM SAHB$_A$(R153D). (**B**) BIM SAHB$_A$ (0–10 μM) likewise triggers BAX activation, as monitored by BAX immunoprecipitation using the 6A7 antibody, which selectively recognizes BAX's N-terminal activation epitope. R153D mutagenesis abrogates the effect. (**C**) A Wright-Giemsa stain of BIM SAHB$_A$–treated OCI-AML3 cells (5 μM) revealed cellular shrinkage, chromatin condensation and marginalization, and nuclear fragmentation, all hallmark morphological features of apoptosis induction (arrowheads). Vehicle- and BIM SAHB$_A$(R153D)–treated cells showed no such effects. Original magnification, ×100; third column, additional ×15 zoom. (**D**) BIM SAHB$_A$ (25 mg/kg/d i.v.) suppressed tumor growth compared with vehicle (n = 7 per arm; 2-way ANOVA, P = 0.018), as assessed by in vivo bioluminescence imaging of a subcutaneous OCI-AML3 tumor xenograft model. Data are mean ± SEM. *P < 0.05.

tal Figure 8, A and B). An analogous study performed with WT B6/129 mice showed equivalent spleen weights across the vehicle, BIM SAHB$_A$, and BIM SAHB$_A$(R153D) treatment groups (Supplemental Figure 8, C and D). In addition, no suppressive effects on peripheral white blood cell counts or peripheral or splenic lymphocyte subsets were detected in the WT mice (Supplemental Figure 9). Thus, we find that BIM SAHB$_A$ triggered cell death of deregulated *Bim*$^{-/-}$ immune cells in a BH3 sequence–specific manner and spared normal host tissues, highlighting the potential of this BIM BH3 replacement strategy to surmount pathologic apoptotic blockades in vivo.

Discussion

To achieve a survival advantage, cancer cells overexpress antiapoptotic BCL-2 family proteins (39) and neutralize the proapoptotic members by interaction-mediated sequestration (40, 41) and/or genetic deletion (14, 15, 42, 43). Targeted pharmacologic strategies to reactivate apoptosis in cancer have focused on inhibiting individual (32) or subsets (4, 5, 44, 45) of BCL-2 family antiapoptotic proteins. Relapsed and refractory cancer, however, is often characterized by the emergence of apoptotic blockade reinforcements that derive from (a) a surge in expression of alternate antiapoptotic proteins or (b) genetic silencing/deletion of proapoptotic proteins, such as the BH3-only subclass. In this context, multimodal targeting of the BCL-2 family pathway with agents designed to block all antiapoptotic proteins, directly trigger the multidomain death proteins, and even pharmacologically replace the death functionality of deleted BH3-only proteins, may be ideally suited to confront chemoresistant disease.

The BH3-only protein BIM has emerged as the most potent death sentinel, engaging all antiapoptotic targets (8, 9, 12) and directly triggering the multidomain proapoptotic proteins (10,

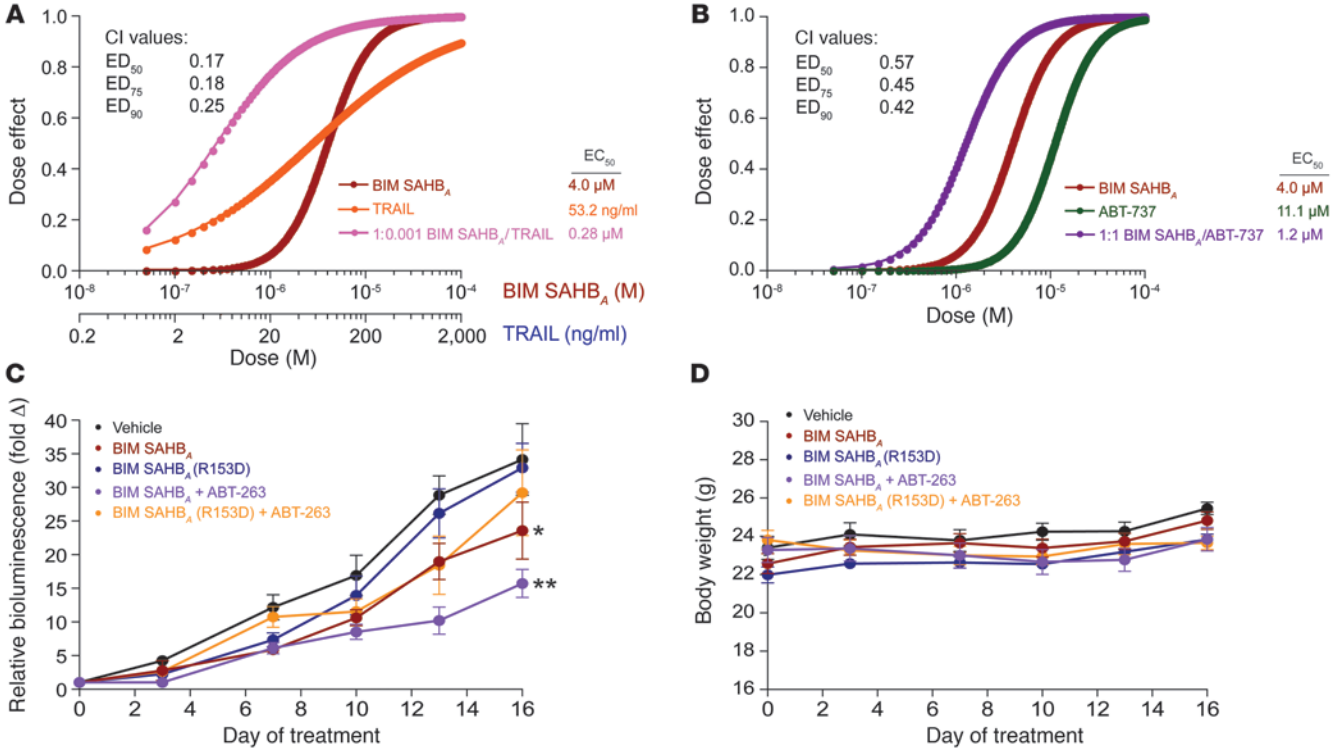

Figure 7

Antitumor activity of combination treatment with BIM SAHB$_A$. Treatment of OCI-AML3 cells with the combination of (**A**) BIM SAHB$_A$/TRAIL or (**B**) BIM SAHB$_A$/ABT-737 caused a synergistic decrease in cell viability, as reflected by CalcuSyn analysis and the plotted dose-effect curves (combination index [CI] <1). EC$_{50}$, 50% effective concentration; ED$_{75}$, 75% effective dose; ED$_{90}$, 90% effective dose. (**C**) The combination of BIM SAHB$_A$ (25 mg/kg/d i.v.) and ABT-263 (100 mg/kg/d PO) caused the most significant suppression of OCI-AML3 tumor growth in vivo, as assessed by in vivo bioluminescence imaging. Two-way ANOVA, overall $P = 0.0052$. Vehicle versus: BIM SAHB$_A$, $P = 0.0299$; BIM SAHB$_A$(R153D), $P = 0.3934$; BIM SAHB$_A$ and ABT-263, $P = 0.0009$; and BIM SAHB$_A$(R153D) and ABT-263, $P = 0.1982$. Data are mean ± SEM ($n = 8$ per arm). *$P < 0.05$; **$P < 0.01$ (**D**) No weight loss manifested among the 5 treatment cohorts over the 16-day observation period. Data are mean ± SEM ($n = 8$ per arm).

11, 19, 46). Thus, we generated a structurally reinforced and cell permeable stapled BIM BH3 helix to maximally reactivate the BCL-2 family death pathway in resistant cancer. We found that BIM SAHB$_A$ binds to a diversity of antiapoptotic and proapoptotic targets with high affinity and potently triggers BAX- and BAK-dependent mitochondrial apoptosis in vitro. In a cellular context, BIM SAHB$_A$ dissociates inhibitory heterodimeric interactions between antiapoptotic and proapoptotic proteins, such as MCL-1/BAK, and triggers conformational activation of the proapoptotic effector protein BAX. Consistent with these biochemical changes induced by low micromolar dosing, BIM SAHB$_A$ dose responsively impairs the viability of hematologic cancer cells, promoting annexin V binding, caspase-3/7 activation, and the morphologic features of apoptosis. Combining BIM SAHB$_A$ with an extrinsic or intrinsic apoptotic pathway stimulant caused synergistic cancer cell death, highlighting the potential utility of BIM SAHB$_A$ in lowering the apoptotic threshold to enhance the cytotoxicity of chemotherapeutic agents. Importantly, BIM SAHB$_A$ imposes preferential toxicity upon cancer cells, as no significant changes in viability were observed for human and murine fibroblasts subjected to BIM SAHB$_A$ treatment at the same micromolar dosing levels.

In the in vivo context, as a single agent and in combination with ABT-263, BIM SAHB$_A$ suppressed tumor growth in a xenograft model of human AML. In addition, BIM SAHB$_A$ selectively restored the death pathway in tissue-infiltrating *Bim*$^{-/-}$ immune cells. Single point mutagenesis of the BIM SAHB$_A$ helical binding surface abrogated death-inducing activity, and no acute toxicity was observed in normal tissues, highlighting the specificity of action of BIM SAHB$_A$. Interestingly, the therapeutic window observed for this and other BCL-2 family modulators (4, 20, 44) appears to derive from the antiapoptotic reserve of unstressed cells, which sustain targeted activation of the BCL-2 family pathway by deploying their natural reservoir of antiapoptotics to bind and sequester activated proapoptotic proteins. In contrast, diseased cells whose antiapoptotic reserve is taxed by tonic death signaling are unable to withstand further BAX/BAK-mediated mitochondrial assault, making them preferentially susceptible to the apoptotic trigger (8). Thus, multimodal targeting of the BCL-2 family pathway through combined antiapoptotic inhibition, direct proapoptotic activation, and pharmacologic replacement of genetically deleted BH3 functionalities may unmask a critical opportunity to overturn the apoptotic blockades of relapsed and refractory cancer and achieve a durable clinical remission.

Methods

SAHB synthesis and characterization. SAHBs were synthesized, derivatized, purified, stored, reconstituted, and characterized by circular dichroism as described in detail previously (20, 47). All peptides were purified by liquid

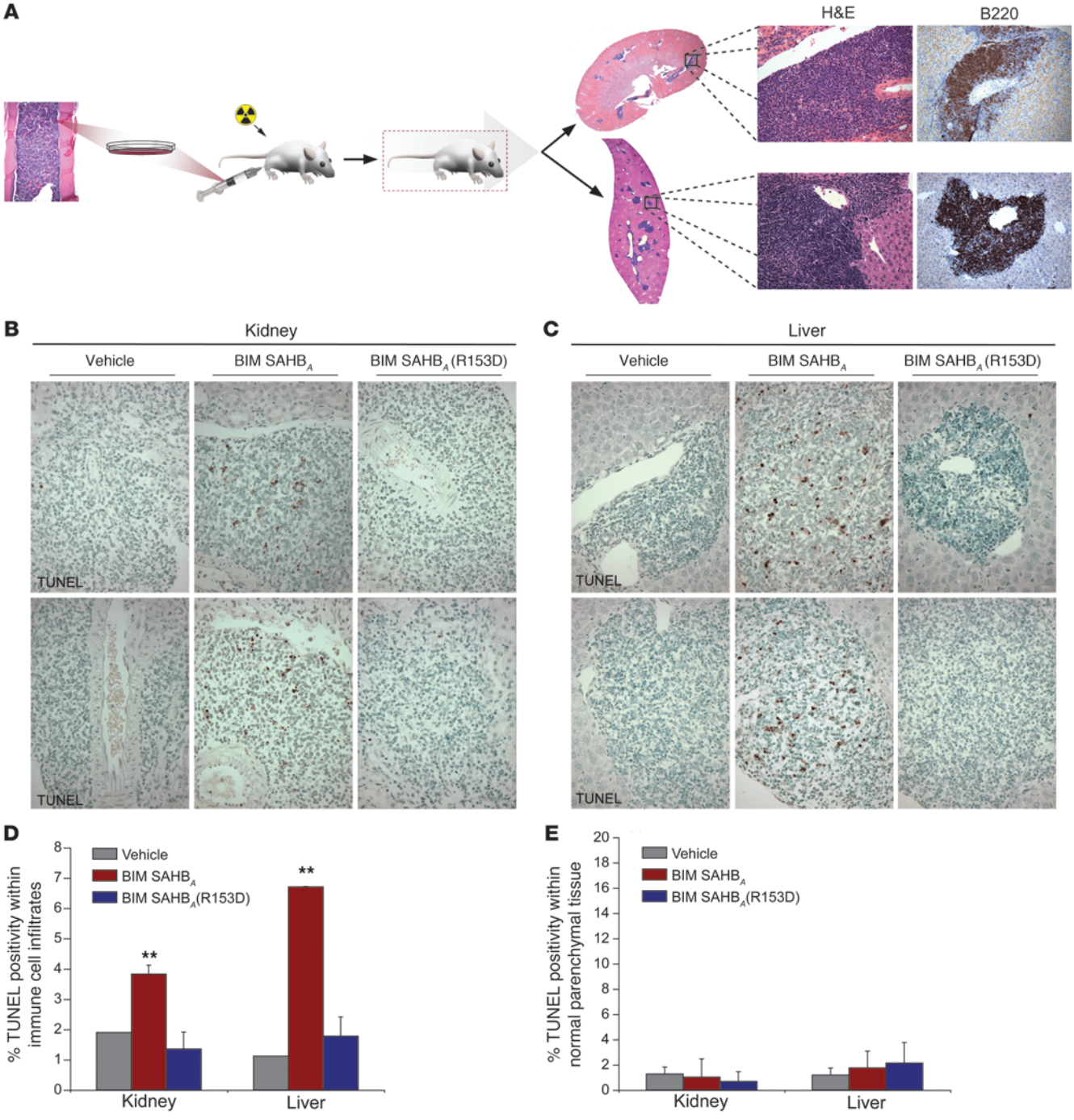

Figure 8

Pharmacologic replacement of BIM BH3 restores the death pathway in *Bim*$^{-/-}$ immune cell infiltrates. (**A**) The infiltrative B cell disease of *Bim*$^{-/-}$ mice was recapitulated in irradiated *Rag2*$^{-/-}$*gc*$^{-/-}$ mice transplanted with the bone marrow of *Bim*$^{-/-}$ mice. Histologic analysis by H&E stain and anti-B220 immunohistochemistry at 19 weeks post transplant revealed extensive B cell infiltration of solid organs. Original magnification: ×2 (whole organs); ×40 (H&E), ×20 (B220 immunohistochemistry). (**B** and **C**) Increased TUNEL staining was evident in the aberrant infiltrates of BIM SAHB$_A$–treated mice as compared with that in vehicle- and BIM SAHB$_A$(R153D)–treated animals. Importantly, the observed increase in TUNEL positivity in BIM SAHB$_A$–treated mice appeared restricted to the deregulated B cells and was not evident in the normal parenchymal tissue. Original magnification, ×100. (**D**) The percentage TUNEL positivity within the immune cell infiltrates was calculated by counting approximately 6,000 cells per 5-μm tissue section from each experimental animal (n = 4 per cohort) in a blinded fashion. A statistically significant increase in percentage of TUNEL positivity was observed in the kidney (P = 0.007) and liver (P = 0.0007) infiltrates of BIM SAHB$_A$–treated mice, an effect that was abrogated by R153D point mutagenesis. Data are mean ± SD. **P < 0.01. (**E**) Importantly, no increase in the number of TUNEL-positive cells was found in kidney and liver parenchymal tissue devoid of the infiltrates. Data are mean ± SD.

chromatography/mass spectrometry to more than 95% purity and quantified by amino acid analysis. The primary sequence compositions of all SAHBs used in this study are listed in Supplemental Table 1. To examine cellular uptake, nonadherent hematologic cancer cells (2×10^6 cells) and adherent fibroblasts (4×10^5 fibroblasts plated 48 hours prior to testing) were incubated with vehicle or BIM BH3 peptides (1 μM) in Opti-MEM (Invitrogen) at 37°C for 2 hours in the dark. Cells were washed with PBS (Invitrogen) and then incubated with 0.25% trypsin (Invitrogen) for 5 minutes at 37°C, washed again with PBS, and incubated on ice in lysis buffer (50 mM Tris [pH 7.4], 150 mM NaCl, 1 mM EDTA, 1 mM DTT, 1% [v/v] Triton X-100, complete protease inhibitor tablet [Roche]). Cellular debris was pelleted at 14,000 *g* for 10 minutes at 4°C, and the supernatant was collected, electrophoresed, and subjected to fluorescence imaging using a Typhoon 9400 (GE Healthcare Life Sciences). To monitor the solution state of BIM SAHBs, lyophilized peptides were resuspended in aqueous buffer containing 50 mM Tris and 100 mM NaCl (pH 8) to generate a 200 μM solution, which was subjected to FPLC analysis using a Superdex-75 column (Amersham Pharmacia) and molecular weight standards (GE Healthcare).

Protein production. Recombinant and tagless BCL-X_LΔC, MCL-1ΔNΔC, BCL-wΔC, and BFL-1/A1ΔC were produced and purified as described previously (19, 32). Briefly, glutathione-S-transferase fusion proteins were expressed in *Escherichia coli* BL21 (DE3) using pGEX2T (Pharmacia Biotech) constructs. Bacterial cells were cultured in ampicillin-containing Luria Broth, and protein expression was induced with 0.5 mM isopropyl β-D-1-thiogalactopyranoside. The bacterial pellet was resuspended in PBS containing 1 mg/ml lysozyme, complete protease inhibitor tablet, and 1% (v/v) Triton X-100 and sonicated, and, after centrifugation at 45,000 *g* for 45 minutes, the supernatant was applied to a glutathione-agarose (Sigma-Aldrich) column and washed with PBS. Tagless protein was obtained by overnight on-bead digestion with thrombin (50 units) (GE Healthcare) in PBS (3 ml) at room temperature, and the cleaved proteins were purified by size exclusion chromatography using 150 mM NaCl and 50 mM Tris (pH 7.4) buffer conditions. Full-length recombinant BAX protein was expressed as previously described (10), and pure monomeric protein was obtained by size exclusion chromatography using a Superdex-75 column (GE Healthcare) and 20 mM HEPES (pH 7.2) and 150 mM KCl buffer conditions.

FP binding assay. FP assays were performed as previously described (19, 48). FITC-BIM $SAHB_A$ and FITC-BIM $SAHB_A$(R153D) (25 nM) were incubated with serial dilutions of recombinant protein in binding buffer (50 mM Tris, 100 mM NaCl [pH 8.0]) until equilibrium was reached. For competition assays, FITC-BAX $SAHB_A$ and FITC-BAK $SAHB_A$ (25 nM) were incubated with BCL-X_LΔC and MCL-1ΔNΔC (100 nM), respectively, in binding buffer for 10 minutes at room temperature. Serial dilutions of acetylated BIM $SAHB_A$ peptides were then added and incubated in the dark at room temperature until equilibrium was reached. FP was measured using a SpectraMax M5 microplate reader (Molecular Devices). For direct binding experiments, dissociation constants (K_d) were calculated by nonlinear regression analysis of dose-response curves using Prism software (GraphPad) (48). For competition experiments, IC_{50} values were determined by nonlinear regression analysis of dose-response curves using a one-site competition model (Graphpad).

Liposomal release assay. Large unilamellar vesicles (LUVs) were generated from a lipid mixture containing 48% phosphatidylcholine, 28% phosphatidylethanolamine, 10% phosphatidylinositol, 10% dioleoyl phosphatidylserine, and 4% tetraoleoyl cardiolipin (Avanti Polar Lipids), as described previously (49). Briefly, the lipid mixture (1 mg aliquots) was prepared from chloroform stocks and dried as a thin film in glass test tubes under nitrogen gas and then under vacuum for 15 hours. Lipids were reconstituted with 45 mM DPX (Invitrogen) and 12.5 mM ANTS (Invitrogen) in 10 mM HEPES (pH 7.0), 200 mM KCl, and 1 mM $MgCl_2$. The lipid suspensions were freeze-thawed 10 times and extruded 11 times through a polycarbonate membrane (100-nm pore size; Avestin) using an extruder (Avanti Polar Lipids), resulting in the generation of LUVs. LUVs were isolated from free DPX/ANTS by gel filtration chromatography using a 10-ml Sepharose CL2B column (GE Healthcare). Liposomal release was quantified based on the increase in fluorescence that occurs when the ANTS fluorophore is separated from the DPX quencher upon release from the liposomes into the supernatant (excitation 355 nm; emission 520 nm; 20-nm bandwidths). Monomeric full-length human BAX protein was purified as described above. LUVs (10 μl) were treated with BAX (400 nM) and SAHBs (200 nM, 400 nM), singly and in combination, in 96-well format (Corning) in a total reaction volume of 100 μl. To evaluate the inhibitory capacity of antiapoptotic BCL-2 family proteins, recombinant BCL-X_LΔC, MCL-1ΔNΔC, BCL-wΔC, and BFL-1/A1ΔC (400 nM) were preincubated with BIM $SAHB_A$ (400 nM) for 20 minutes and then treated with BAX (400 nM) and LUVs (10 μl) in 96-well format in a total reaction volume of 100 μl. Fluorescence (F) was measured from $t = 0$ (F0) to $t = 2$ hours, and then Triton X-100 was added to a final concentration of 0.2% (v/v), followed by measurement of fluorescence for an additional 10 minutes to determine maximal release (F100). The percentage ANTS/DPX release was calculated with the following formula: ([F – F0]/[F100 – F0]) × 100.

Cytochrome c release assay. MLM (0.5 mg/ml) were isolated from WT and *Alb-cre^{pos}Bax$^{fl/-}$Bak$^{-/-}$* mice as described previously (19, 48) and incubated with the indicated BCL-2 family proteins and SAHB ligands at 37°C for 40 minutes. The pellet and supernatant fractions were isolated by centrifugation, and cytochrome *c* was quantitated using a colorimetric ELISA assay (R&D Systems). The percentage cytochrome *c* released into the supernatant from releasable mitochondrial pools (%cyto*c*) was calculated according to the following equation: $\%cyto c = [(cyto c_{sup} - cyto c_{backgr})/(cyto c_{total} - cyto c_{backgr})] \times 100$, where $cyto c_{sup}$, $cyto c_{backgr}$, and $cyto c_{total}$ represent cytochrome *c* detected in the supernatants of SAHB-, vehicle-, and 1% Triton-X 100–treated samples, respectively.

Cell culture. OCI-AML3, U937, OPM-2, Pfeiffer, and K562 cells were maintained in RPMI 1640 media (Invitrogen) supplemented with 10% FBS, 100 U ml^{-1} penicillin/streptomycin, 2 mM L-glutamine, 50 mM HEPES, 0.1 mM MEM nonessential amino acids, and 50 μM β-mercaptoethanol. WT and DKO MEFs were maintained in DMEM (Invitrogen) supplemented with 10% FBS, 100 U ml^{-1} penicillin/streptomycin, 2 mM L-glutamine, 0.1 mM MEM nonessential amino acids, and 50 μM β-mercaptoethanol. WS1 fibroblasts were maintained in EMEM (ATCC) supplemented with 10% FBS, 100 U ml^{-1} penicillin/streptomycin, 2 mM L-glutamine, 1 mM sodium pyruvate, and 0.1 mM MEM nonessential amino acids.

Live cell confocal microscopy. Cells were incubated with 1 μM FITC-BIM SAHBs for 2 hours in Opti-MEM media lacking phenol red (Invitrogen), followed by 30 minutes of incubation in prewarmed Opti-MEM solution containing 50 nM MitoTracker Red (Invitrogen) and 5 μg/ml Hoechst 33342 (Invitrogen). The cells were then washed twice and plated on glass bottom poly-D-lysine–coated culture dishes (MatTek Corporation) in Opti-MEM media lacking phenol red (Invitrogen). Confocal images were collected on a Yokogawa CSU-X1 spinning disk confocal system (Andor Technology) attached to a Nikon Ti-E inverted microscope (Nikon Instruments). Excitation of the 3 fluorophores was performed sequentially using the 405-nm, 488-nm, and 561-nm lasers. Images were acquired using a ×100 Plan Apo objective lens with a Hamamatsu OrcaER camera (Hamamatsu Photonics). Acquisition parameters, shutters, filter positions, and focus were controlled by Andor iQ software (Andor Technology).

Cell viability assay. Cancer cells (1×10^4 cells, 50 μl) were aliquoted in 96-well opaque plates and treated with serial dilutions of vehicle (0.2% DMSO), BIM $SAHB_A$, or BIM $SAHB_A$(R153D) in serum-free RPMI media for 2 hours, followed by serum replacement with 20% FBS-containing RPMI

media (50 μl) for a final volume of 100 μl containing 10% FBS. Cell viability was assayed at 24 hours by addition of CellTiter-Glo chemiluminescence reagent (Promega), and luminescence measured by a SpectraMax M5 microplate reader (Molecular Devices). For adherent fibroblasts, WS1 (2.5×10^3) and WT (2.5×10^3) and DKO (1.5×10^3) cells were plated in their respective culture media (see above), and, 24 hours later (~75%–90% cellular confluence), media was removed and the cells were washed with the corresponding serum-free media. The indicated doses of SAHB were then added in serum-free media (50 μl), serum was replaced after 2 hours (20% FBS-containing media, 50 μl), and cell viability was measured at 24 hours as above. For synergy analyses, OCI-AML3 cells (1×10^4 cells) were treated with serial dilutions of BIM $SAHB_A$ (0.01–20 μM), human TRAIL (0.2–200 ng/ml; R&D systems), ABT-737 (0.01–20 μM; Selleck), or the BIM $SAHB_A$/TRAIL and BIM $SAHB_A$/ABT-737 combinations. Cell viability was measured at 24 hours by CellTiter-Glo, according to the manufacturer's protocol. Synergy analyses were then performed using CalcuSyn software (35).

Annexin V binding. Cancer cells (5×10^4 cells) were treated with SAHBs as above, washed with PBS and annexin V binding buffer after 6 hours, and then incubated with FITC–annexin V (BD Pharmingen) for 20 minutes at room temperature in the dark, as described previously (48). Cells were then washed with binding buffer and analyzed by flow cytometry on a FACS-Calibur (Becton Dickinson), and the percentage annexin V positivity was calculated using FlowJo software.

Caspase-3/7 activation assay. Cancer cells and fibroblasts were treated with SAHBs as described above for cell viability assays, and caspase-3/7 activation was measured at 6 hours by addition of the Caspase-Glo 3/7 chemiluminescence reagent in accordance with the manufacturer's protocol (Promega). Luminescence was detected by a SpectraMax M5 microplate reader (Molecular Devices).

Immunoprecipitation. To monitor the MCL-1/BAK complex, OCI-AML3 cells (5×10^6 cells) were incubated with vehicle, BIM $SAHB_A$, or BIM $SAHB_A$(R153D) at the indicated concentrations in Opti-MEM media at 37°C for 2 hours, followed by PBS wash at 4°C, and incubation on ice in 200 μl lysis buffer (50 mM Tris [pH 7.4], 150 mM NaCl, 1 mM EDTA, 1 mM DTT, 0.5% [v/v] NP-40, complete protease inhibitor tablet). After 15 minutes, cellular debris was pelleted at 14,000 *g* for 10 minutes at 4°C, and the supernatant was collected and incubated with pre-equilibrated protein A/G sepharose beads (Santa Cruz Biotechnology Inc.). The precleared supernatant was then incubated with anti–MCL-1 antibody (4 μg/ml) (S-19, Santa Cruz Biotechnology Inc.) overnight at 4°C, followed by the addition of pre-equilibrated protein A/G sepharose beads for 1 hour. The beads were pelleted, washed with lysis buffer 3 times at 4°C, and protein eluted by heating the beads at 90°C for 10 minutes in LDS/DTT loading buffer. The immunoprecipitates were subjected to electrophoresis and Western blot analysis using anti-BAK (1:500) (NT, CalBiochem) and anti–MCL-1 (1:200) (S-19, Santa Cruz Biotechnology Inc.) antibodies. For detection of activated BAX, OCI-AML3 cells (2.5×10^6 cells) were treated as above, except that a CHAPS-based buffer was used for cellular lysis (10 mM HEPES [pH 7.4], 150 mM NaCl, 1% [w/v] CHAPS, complete protease inhibitor tablet). Lysates were precleared as above, protein concentrations were determined by Bradford assay (Bio-Rad Protein Assay), and 500 μg of precleared lysate was incubated overnight with the 6A7 anti-BAX antibody (6 μg/ml) (Santa Cruz Biotechnology Inc.) at 4°C, followed by addition of pre-equilibrated protein A/G sepharose beads for 2 hours. The beads were pelleted, washed 5 times in CHAPS lysis buffer at 4°C, and protein eluted by heating at 90°C for 10 minutes in LDS/DTT loading buffer. The immunoprecipitates were subjected to electrophoresis and Western blot analysis using anti-BAX antibody (1:2,000) (N20, Santa Cruz Biotechnology Inc.).

Wright-Giemsa stain. OCI-AML3 cells (2.5×10^6 cells) were treated with vehicle or BIM SAHBs at the indicated concentrations in Opti-MEM media for 4 hours at 37°C. Cells were collected and washed twice with PBS containing 2% FBS and resuspended at 2.5×10^6 cells/ml for mounting of the cellular suspension (100 μl) onto glass slides by cytospin (Cytospin3, Shandon). The slides were air dried and then stained with Accustain Modified Wright-Giemsa according to the manufacturer's protocol (Sigma-Aldrich).

OCI-AML3 xenograft and in vivo efficacy study. Six-week-old female NSG mice were purchased from The Jackson Laboratory and acclimated for 1 week prior to tumor cell inoculation. OCI-AML3-LucNeo cells (5×10^6 cells) were injected subcutaneously with 30% matrigel into the right hind flank. In vivo bioluminescence imaging was conducted after injection of 75 mg/kg of D-luciferin (Promega) using a Xenogen IVIS Spectrum (Caliper Life Sciences). Eight days after inoculation, mice with equivalent disease, as determined by bioluminescence imaging, were divided into 2 groups ($n = 8$ per arm) and treated with the indicated agent, route, and duration. The diluent was 5% DMSO/D5W for BIM SAHB and 60% Phosal/30% PEG-400/10% ethanol for ABT-263. Tumor burden was monitored by serial bioluminescence imaging and quantified using the Living Images software package (Caliper Life Sciences).

$Bim^{-/-}$ bone marrow transplantation and in vivo efficacy study. $Rag2^{-/-}gc^{-/-}$ mice (20 weeks old; Taconic) were subjected to irradiation (900 cGy; Gammacell-40 Exactor irradiator, Theratronics) and tail vein infusion of 2×10^6 bone marrow cells harvested from the femurs and tibias of 16-week-old $Bim^{+/+}$ or $Bim^{-/-}$ mice (37). The spleens of $Bim^{+/+}$ and $Bim^{-/-}$ mice (18–20 weeks old) and of mock, $Bim^{+/+}$, and $Bim^{-/-}$ bone marrow–reconstituted $Rag2^{-/-}gc^{-/-}$ mice (12 weeks post transplant) were imaged by micro-ultrasound (Vevo 770 system, VisualSonics) to evaluate splenomegaly. Mice were injected intraperitoneally with Avertin (10 g tribromoethanol and 10 ml tertiary amyl alcohol [Sigma-Aldrich]) at a dose of 0.015 ml/g body weight, followed by removal of abdominal hair with electric clippers and depilatory cream (Nair). Medical ultrasound acoustic gel was applied to the abdomen and ultrasound imaging was performed, followed by calculation of spleen volumes using the Vevo 770 imaging software. To assess for hypergammaglobulinemia, blood was withdrawn from $Bim^{+/+}$ and $Bim^{-/-}$ mice (18–20 weeks old) and $Bim^{-/-}$ bone marrow–reconstituted $Rag2^{-/-}gc^{-/-}$ mice (15 weeks post transplant) by retro-orbital bleed, and serum Ig titers were quantified using the mouse immunoglobin isotyping ELISA system (BD Pharmingen) according to the manufacturer's protocol. Serum samples were diluted by 1:10,000–1:100,000 depending on the isotype, such that absorbance readings were measured in the linear range of Ig controls. For in vivo efficacy analysis, 3 cohorts ($n = 4$) of post transplant day–matched, $Bim^{-/-}$ bone marrow–reconstituted, $Rag2^{-/-}gc^{-/-}$ mice were treated with once daily tail vein injections of vehicle (5% DMSO/D5W), BIM $SAHB_A$ (10 mg/kg), or BIM $SAHB_A$(R153D) (10 mg/kg) for 5 days. Twenty-four hours after the final injection, the mice were euthanized by CO_2 asphyxiation. Animals and excised spleens were weighed, and tissues were harvested for fixation in 10% buffered formalin (Fisher Scientific). Paraffin-embedded sections (5 μm) were stained with H&E or subjected to immunohistochemistry (Specialized Histopathology Service, Brigham and Women's Hospital). For immunohistochemistry, slides were soaked in xylene, passed through graded alcohols, immersed in distilled water, and treated with either EDTA or 10 mM citrate (pH 6.0) (Zymed Laboratories) in a steam pressure cooker (Decloaking Chamber, BioCare Medical) according to the manufacturer's instructions and then washed in distilled water. All subsequent steps were performed at room temperature in a hydrated chamber. Slides were treated with Peroxidase Block (DakoCytomation) for 5 minutes to quench endogenous peroxidase activity and then primary monoclonal B220 antibody (1:200) (DakoCytomation) applied in DakoCytomation diluent for 1 hour. Slides were washed in 50 mM Tris-Cl (pH 7.4), and a rabbit anti-rat antibody was applied for 30 minutes. To develop the slides, an anti-rabbit HRP-conjugated antibody (Envision

Detection Kit, DakoCytomation) was applied for 30 minutes, followed by washing, immunoperoxidase staining with the Diaminobenzidine Chromogen Kit (DakoCytomation), and hematoxylin counterstaining. TUNEL staining was performed using the ApopTag Peroxidase ISOL Apoptosis Detection Kit (Millipore) in accordance with the manufacturer's protocol. Slides were analyzed using an Olympus BX50 microscope equipped with an Olympus Qcolor5 digital photo camera and images downloaded to Adobe Photoshop software. The percentage of TUNEL-positive lymphocytes within the infiltrates was calculated by counting approximately 6,000 lymphocytes per 5-μm section per animal in blinded fashion using pictures of random ×40 fields ([TUNEL-positive cells/total cells counted] × 100). The number of TUNEL-positive cells per ×20 field of infiltrate-free tissue (~40 fields of kidney tissue and ~60 fields of liver tissue within a 5-μm section per animal) was counted to determine background TUNEL positivity within the normal parenchyma. Statistical significance was calculated using the 2-tailed Student's *t* test. For comparative cytotoxicity analysis, 3 cohorts (n = 4 per arm) of 15- to 16-week-old WT B6/129 mice (Taconic), reflecting the same mixed background upon which the *Bim*$^{-/-}$ mice were generated (37), were treated with vehicle, BIM SAHB$_A$, or BIM SAHB$_A$(R153D) as above. Prior to the study and 24 hours after the last injection, blood was collected by retro-orbital bleed and subjected to cell counting (ADVIA 2120i, Siemens Healthcare Diagnostics Inc.). In addition, peripheral blood and splenocytes were analyzed by flow cytometry (FACSCalibur, Becton Dickinson) using the following monoclonal antibodies (BD Pharmingen) conjugated to FITC, PE, or APC: GK1.5 (anti-CD4), 53-6.7 (anti-CD8), and RA3-6B2 (anti-B220). FACS data were analyzed using FlowJo software (Tree Star Inc.).

Statistics. Statistical significance was determined by 2-tailed Student's *t* test for pair-wise comparison of groups. Two-way repeated-measures ANOVA with Bonferroni correction was used for comparisons of 2 or more groups over a time course. P values of less than 0.05 were considered significant.

Study approval. All animal experiments were approved by and performed in accordance with the guidelines and regulations set forth by the Institutional Animal Care and Use Committee of the Dana-Farber Cancer Institute.

Acknowledgments

We thank E.D. Smith, A.L. Christie, and L. Cameron for assistance with graphics, animal treatment and imaging, and confocal microscopy, respectively. This work was supported by a Lauri Strauss Leukemia Foundation Discovery Grant, a Leukemia and Lymphoma Society Special Fellow Award, and NIH grant 1K08CA151450 to J.L. LaBelle and NIH grants 5P01CA92625 and 5R01CA050239, a Leukemia and Lymphoma Society SCOR grant, the Todd J. Schwartz Pediatric Oncology Fund, a grant from the Wolpoff Family Foundation, and a Burroughs Wellcome Fund Career Award to L.D. Walensky. We thank the LaTorre family for their generous support of C. Lawrence.

Received for publication March 5, 2012, and accepted in revised form April 4, 2012.

Address correspondence to: Loren D. Walensky, Dana-Farber Cancer Institute, 450 Brookline Avenue, Mayer 664, Boston, Massachusetts 02215, USA. Phone: 617.632.6307; Fax: 617.582.8240; E-mail: loren_walensky@dfci.harvard.edu.

1. Danial NN, Korsmeyer SJ. Cell death: critical control points. *Cell*. 2004;116(2):205–219.
2. Tait SW, Green DR. Mitochondria and cell death: outer membrane permeabilization and beyond. *Nat Rev Mol Cell Biol*. 2010;11(9):621–632.
3. Sattler M, et al. Structure of Bcl-xL-Bak peptide complex: recognition between regulators of apoptosis. *Science*. 1997;275(5302):983–986.
4. Oltersdorf T, et al. An inhibitor of Bcl-2 family proteins induces regression of solid tumours. *Nature*. 2005;435(7042):677–681.
5. Tse C, et al. ABT-263: a potent and orally bioavailable Bcl-2 family inhibitor. *Cancer Res*. 2008;68(9):3421–3428.
6. Konopleva M, et al. Mechanisms of apoptosis sensitivity and resistance to the BH3 mimetic ABT-737 in acute myeloid leukemia. *Cancer Cell*. 2006;10(5):375–388.
7. van Delft MF, et al. The BH3 mimetic ABT-737 targets selective Bcl-2 proteins and efficiently induces apoptosis via Bak/Bax if Mcl-1 is neutralized. *Cancer Cell*. 2006;10(5):389–399.
8. Certo M, et al. Mitochondria primed by death signals determine cellular addiction to antiapoptotic BCL-2 family members. *Cancer Cell*. 2006;9(5):351–365.
9. Chen L, et al. Differential targeting of prosurvival Bcl-2 proteins by their BH3-only ligands allows complementary apoptotic function. *Mol Cell*. 2005;17(3):393–403.
10. Gavathiotis E, et al. BAX activation is initiated at a novel interaction site. *Nature*. 2008; 455(7216):1076–1081.
11. Kuwana T, et al. BH3 domains of BH3-only proteins differentially regulate Bax-mediated mitochondrial membrane permeabilization both directly and indirectly. *Mol Cell*. 2005;17(4):525–535.
12. Merino D, et al. The role of BH3-only protein Bim extends beyond inhibiting Bcl-2-like prosurvival proteins. *J Cell Biol*. 2009;186(3):355–362.
13. Inomata M, Tagawa H, Guo YM, Kameoka Y, Takahashi N, Sawada K. MicroRNA-17-92 downregulates expression of distinct targets in different B-cell lymphoma subtypes. *Blood*. 2009; 113(2):396–402.
14. Mestre-Escorihuela C, et al. Homozygous deletions localize novel tumor suppressor genes in B-cell lymphomas. *Blood*. 2007;109(1):271–280.
15. Tagawa H, et al. Genome-wide array-based CGH for mantle cell lymphoma: identification of homozygous deletions of the proapoptotic gene BIM. *Oncogene*. 2005;24(8):1348–1358.
16. Kashiwagi H, et al. TAT-Bim induces extensive apoptosis in cancer cells. *Ann Surg Oncol*. 2007;14(5):1763–1771.
17. Kazi A, et al. The BH3 alpha-helical mimic BH3-M6 disrupts BCL-XL, BCL-2 and MCL-1 protein-protein interactions with BAX, BAK, BAD or BIM and induces apoptosis in a BAX- and BIM-dependent manner. *J Biol Chem*. 2011;286(11):9382–9392.
18. Ponassi R, et al. A novel Bim-BH3-derived Bcl-XL inhibitor: biochemical characterization, in vitro, in vivo and ex-vivo anti-leukemic activity. *Cell Cycle*. 2008;7(20):3211–3224.
19. Walensky LD, et al. A stapled BID BH3 helix directly binds and activates BAX. *Mol Cell*. 2006; 24(2):199–210.
20. Walensky LD, et al. Activation of apoptosis in vivo by a hydrocarbon-stapled BH3 helix. *Science*. 2004;305(5689):1466–1470.
21. Fire E, Gulla SV, Grant RA, Keating AE. Mcl-1-Bim complexes accommodate surprising point mutations via minor structural changes. *Protein Sci*. 2010;19(3):507–519.
22. Herman MD, et al. Completing the family portrait of the anti-apoptotic Bcl-2 proteins: crystal structure of human Bfl-1 in complex with Bim. *FEBS Lett*. 2008;582(25–26):3590–3594.
23. Liu X, Dai S, Zhu Y, Marrack P, Kappler JW. The structure of a Bcl-xL/Bim fragment complex: implications for Bim function. *Immunity*. 2003;19(3):341–352.
24. Gavathiotis E, Reyna DE, Davis ML, Bird GH, Walensky LD. BH3-triggered structural reorganization drives the activation of proapoptotic BAX. *Mol Cell*. 2010;40(3):481–492.
25. Chipuk JE, Fisher JC, Dillon CP, Kriwacki RW, Kuwana T, Green DR. Mechanism of apoptosis induction by inhibition of the anti-apoptotic BCL-2 proteins. *Proc Natl Acad Sci U S A*. 2008;105(51):20327–20332.
26. Kim H, et al. Hierarchical regulation of mitochondrion-dependent apoptosis by BCL-2 subfamilies. *Nat Cell Biol*. 2006;8(12):1348–1358.
27. Willis SN, et al. Apoptosis initiated when BH3 ligands engage multiple Bcl-2 homologs, not Bax or Bak. *Science*. 2007;315(5813):856–859.
28. Deng J, Carlson N, Takeyama K, Dal Cin P, Shipp M, Letai A. BH3 profiling identifies three distinct classes of apoptotic blocks to predict response to ABT-737 and conventional chemotherapeutic agents. *Cancer Cell*. 2007;12(2):171–185.
29. Li G, et al. Effective targeting of STAT5-mediated survival in myeloproliferative neoplasms using ABT-737 combined with rapamycin. *Leukemia*. 2010;24(8):1397–1405.
30. Deng J, et al. Proapoptotic BH3-only BCL-2 family protein BIM connects death signaling from epidermal growth factor receptor inhibition to the mitochondrion. *Cancer Res*. 2007;67(24):11867–11875.
31. Martinou JC, Youle RJ. Mitochondria in apoptosis: Bcl-2 family members and mitochondrial dynamics. *Dev Cell*. 2011;21(1):92–101.
32. Stewart ML, Fire E, Keating AE, Walensky LD. The MCL-1 BH3 helix is an exclusive MCL-1 inhibitor and apoptosis sensitizer. *Nat Chem Biol*. 2010;6(8):595–601.
33. Hsu YT, Youle RJ. Nonionic detergents induce dimerization among members of the Bcl-2 family. *J Biol Chem*. 1997;272(21):13829–13834.
34. Callens C, et al. Targeting iron homeostasis induces cellular differentiation and synergizes with differentiating agents in acute myeloid leukemia. *J Exp Med*. 2010;207(4):731–750.
35. Chou TC. Theoretical basis, experimental design, and computerized simulation of synergism and antagonism in drug combination studies. *Pharm*

Rev. 2006;58(3):621–681.
36. Gandhi L, et al. Phase I study of Navitoclax (ABT-263), a novel Bcl-2 family inhibitor, in patients with small-cell lung cancer and other solid tumors. *J Clin Oncol*. 2011;29(7):909–916.
37. Takeuchi O, Fisher J, Suh H, Harada H, Malynn BA, Korsmeyer SJ. Essential role of BAX,BAK in B cell homeostasis and prevention of autoimmune disease. *Proc Natl Acad Sci U S A*. 2005; 102(32):11272–11277.
38. Bouillet P, et al. Proapoptotic Bcl-2 relative Bim required for certain apoptotic responses, leukocyte homeostasis, and to preclude autoimmunity. *Science*. 1999;286(5445):1735–1738.
39. Tsujimoto Y, Finger LR, Yunis J, Nowell PC, Croce CM. Cloning of the chromosome breakpoint of neoplastic B cells with the t(14;18) chromosome translocation. *Science*. 1984;226(4678):1097–1099.
40. Brunelle JK, Ryan J, Yecies D, Opferman JT, Letai A. MCL-1-dependent leukemia cells are more sensitive to chemotherapy than BCL-2-dependent counterparts. *J Cell Biol*. 2009;187(3):429–442.
41. Letai A, Sorcinelli MD, Beard C, Korsmeyer SJ. Anti-apoptotic BCL-2 is required for maintenance of a model leukemia. *Cancer Cell*. 2004;6(3):241–249.
42. Meijerink JP, et al. Hematopoietic malignancies demonstrate loss-of-function mutations of BAX. *Blood*. 1998;91(8):2991–2997.
43. Egle A, Harris AW, Bouillet P, Cory S. Bim is a suppressor of Myc-induced mouse B cell leukemia. *Proc Natl Acad Sci U S A*. 2004;101(16):6164–6169.
44. Nguyen M, et al. Small molecule obatoclax (GX15-070) antagonizes MCL-1 and overcomes MCL-1-mediated resistance to apoptosis. *Proc Natl Acad Sci U S A*. 2007;104(49):19512–19517.
45. Paoluzzi L, et al. Targeting Bcl-2 family members with the BH3 mimetic AT-101 markedly enhances the therapeutic effects of chemotherapeutic agents in in vitro and in vivo models of B-cell lymphoma. *Blood*. 2008;111(11):5350–5358.
46. Letai A, Bassik MC, Walensky LD, Sorcinelli MD, Weiler S, Korsmeyer SJ. Distinct BH3 domains either sensitize or activate mitochondrial apoptosis, serving as prototype cancer therapeutics. *Cancer Cell*. 2002;2(3):183–192.
47. Bird GH, Bernal F, Pitter K, Walensky LD. Synthesis and biophysical characterization of stabilized alpha-helices of BCL-2 domains. *Methods Enzymol*. 2008;446:369–386.
48. Pitter K, Bernal F, Labelle J, Walensky LD. Dissection of the BCL-2 family signaling network with stabilized alpha-helices of BCL-2 domains. *Methods Enzymol*. 2008;446:387–408.
49. Billen LP, Kokoski CL, Lovell JF, Leber B, Andrews DW. Bcl-XL inhibits membrane permeabilization by competing with Bax. *PLoS Biol*. 2008;6(6):e147.
50. Zong WX, Ditsworth D, Bauer DE, Wang ZQ, Thompson CB. Alkylating DNA damage stimulates a regulated form of necrotic cell death. *Genes Dev*. 2004;18(11):1272–1282.